# Tuneable magneto-optical metamaterials based on photonic resonances in nickel nanorod arrays

Toal, B., McMillen, M., Murphy, A., Hendren, W., Atkinson, R., & Pollard, R. (2014). Tuneable magneto-optical metamaterials based on photonic resonances in nickel nanorod arrays. Materials Research Express, 1(1), [015801]. DOI: 10.1088/2053-1591/1/1/015801

**Published in:**
Materials Research Express

**Document Version:**
Publisher's PDF, also known as Version of record

**Queen's University Belfast - Research Portal:**
Link to publication record in Queen's University Belfast Research Portal

Tuneable magneto-optical metamaterials based on photonic resonances in nickel nanorod arrays



2014 Mater. Res. Express 1 015801

(http://iopscience.iop.org/2053-1591/1/1/015801)

Materials Research
Express

# Tuneable magneto-optical metamaterials based on photonic resonances in nickel nanorod arrays

**Brian Toal, Mark McMillen, Antony Murphy, William Hendren, Ron Atkinson and Robert Pollard**

Queens University Belfast, University Road, Belfast, United Kingdom, BT7 1NN
E-mail: btoal01@qub.ac.uk

Received 11 November 2013, revised 4 December 2013
Accepted for publication 11 December 2013
Published 27 January 2014
*Materials Research Express* **1** (2014) 015801
doi:10.1088/2053-1591/1/1/015801

**Abstract**

We investigate the magneto-optical properties of a nanostructured metamaterial comprised of arrays of nickel nanorods embedded in an anodized aluminum oxide template. The rods are grown using a self-assembly bottom-up technique that provides a uniform, quasi-hexagonal array over a large area, quickly and at low cost. The tuneability of the magneto-optic response of the material is investigated by varying the nanorod dimensions: diameter, length and inter-rod spacing as well as the overall thickness of the template. It is demonstrated that the system acts as a sub-wavelength light trap with enhanced magneto-optical properties occurring at reflectivity minima corresponding to photonic resonances of the metamaterial. Changes in dimensions of the nickel rods on the order of tens of nanometers cause a spectral blue-shift in the peak magneto-optical response of 270 nm in the visible range. A plasmonic enhancement is also observed at lower wavelengths, which becomes increasingly damped with larger diameters and increased volume fraction of nickel inclusions. This type of structure has potential applications in high density magneto-optical data storage (up to $10^{11-12}$ rods per square inch), ultrafast magneto-plasmonic switching and optical components for telecommunications.

Keywords: nanowires, metamaterial, magneto-optics, tuneable, Kerr effect

## Introduction

Metamaterials are artificially constructed materials with enhanced and unique properties that are not seen in nature such as negative index of refraction [1, 2] or epsilon-near-zero (ENZ) [3]. These new materials are already being utilised in both existing and emerging technologies, such as in superlensing [2] and cloaking devices [4], optical microscopy [5], photonic circuits [6, 7] and microwave antennas [8]. In order to achieve effects different from those naturally occurring in materials, functional inclusions, or meta-atoms, of sub wavelength dimensions are used to manipulate incident EM radiation in a desired manner. Metallic nanorods demonstrate a range of interesting properties different from those of their bulk counterparts and metamaterials consisting of magnetic nanorods embedded in a host dielectric enable tailoring of both the optical and ferromagnetic response.

Magnetic nanostructures are of high technological importance in their own right. They are finding applications in high-density data storage [9–11], giant magnetoresistance sensors [12, 13], biomagnetic [14, 15] and medical devices [16], high frequency devices such as microstrip circulators [17] and for tuneable planar microwave integrated circuits [18]. Nowadays there are several techniques for fabricating nanostructures. Some of the more utilized methods include nanolithography [19], self-assembly of colloids using chemical reduction methods [20–22] and electrodeposition into the voids of a nanoporous material such as anodized aluminum oxide (AAO) [23–25] or track-etched polymer membranes [12, 18, 26]. Nanolithography can be used to create arrays of novel shapes such as triangles [27], cones [28, 29] or split-rings [1]. Electrodeposition into AAO templates is a self-assembly technique, capable of creating large scale arrays of uniform nanowires [30].

The magnetic properties of nickel nanowires have mostly been studied in systems that involve an extremely high aspect ratio array of wires (several microns in length), prepared using high purity Aluminum (Al) foils [31–33]. There have also been previous studies that examined the properties of nickel nanowires with aspect ratios as low as 10 to 20 [23]. Below this however, there is a gap in the research until we reach the realm of the nanodiscs with aspect ratios less than one. These structures also show interesting properties. For example, it has been demonstrated that localized surface plasmons (LSPs) can be exploited to achieve a controlled manipulation of the magneto-optical (MO) response of pure nickel nanodiscs [19]. This could potentially lead to faster more efficient high-density magneto-optical storage drives, with the possibility of circularly-polarized light being used to induce magnetization via the inverse Faraday effect [34, 35].

In this work, we bridge the gap between long magnetic nanowires, prepared by electrodeposition, and nanodiscs prepared by e-beam lithography. We demonstrate a large enhancement of magneto-optical response of nickel nanorods with a significant reduction in the aspect ratio (<5) from those previously reported. These metamaterials are effectively high quality optical films demonstrating enhanced magneto-optics in a sub wavelength slab of material. In general, the electromagnetic response of these nanostructured metamaterials can be expressed in terms of homogenized material parameters with uniaxial anisotropy, and can be modeled as such using effective medium theory.

## Experimental

Magnetron sputtering was used to deposit a thin film multilayer of $Ta_2O_5$, Au and Al onto a clean glass substrate. The aluminum is anodized in a 1 °C bath of 0.3 M sulfuric acid at 35 V to create a quasi-hexagonal lattice of nano-porous AAO. The template is then etched in aqueous NaOH to remove the boundary layer which forms at the bottom of the pores. Nickel is electrodeposited into the pores at −1.1 V from a 200 mM, 2.5 pH. nickel sulfate ($NiSO_4(H_2O)_6$) solution. The transparency of the underlayers and AAO at optical wavelength allows us to measure the drop in transmission *in-situ* and control the length of the wires. Longer etching times increase the pores diameter and also lead to shorter wires in our particular set-up, as the samples were prepared on a single substrate and electrodeposited at the same time. Etching in NaOH not only removes AAO from the pore walls but also from the top surface resulting in a thinning of the template for longer etching times. The inter-pore spacing, however, is exclusively determined by the anodizing voltage; for example, 35 V results in a spacing period of 85 nm.

The magneto-optical measurements were all taken in the polar Kerr configuration at normal incidence (less than 3 degrees) using a white light source and monochromator. The field strength is 0.8 T and the wavelength range is 400–880 nm.

## Tuning the geometry

Six different samples were fabricated for this study by electrodeposition of nickel into a porous AAO template. A high degree of tuneability is possible in such metamaterials via control of the nanorod dimensions and inter-rod spacing by varying the deposition conditions. Figure 1(a) shows a schematic of the growth process and highlights the tuneable parameters. The inter-rod spacing can be tuned, between 50 nm and 90 nm, by varying the anodizing voltage. The rod diameter can range from 20 nm to 70 nm depending on how long the alumina is chemically etched. The rod length can be anywhere up to the thickness of the AAO, which is a sputtered film and can be any thickness we require. A full description of the tuneability intrinsic to this fabrication process can be found in [36].

The nanorod geometries chosen for this study are illustrated in figure 1(c). The geometries were obtained via direct measurement on individual rods with the AAO completely removed. Figure 1(b) is an example of a scanning electron micrograph (SEM) from which the measurements are taken. The impression of the rods falling into directions non-perpendicular to the substrate is misleading as all optical measurements are taken with the AAO template in place. This happens as a result of capillary effects during the drying procedure [37]. The template provides structural stability and keeps the rods fully separated and perpendicular to the substrate. The diameter of the nanorods across the six samples increases from 33 nm to 56 nm, and the average length decreases from 160 nm to 100 nm, giving a change in aspect ratio of 4.9 down to 1.8. However, the center to center spacing is kept constant for all samples, so as diameter increases the separation between adjacent rods is reduced.

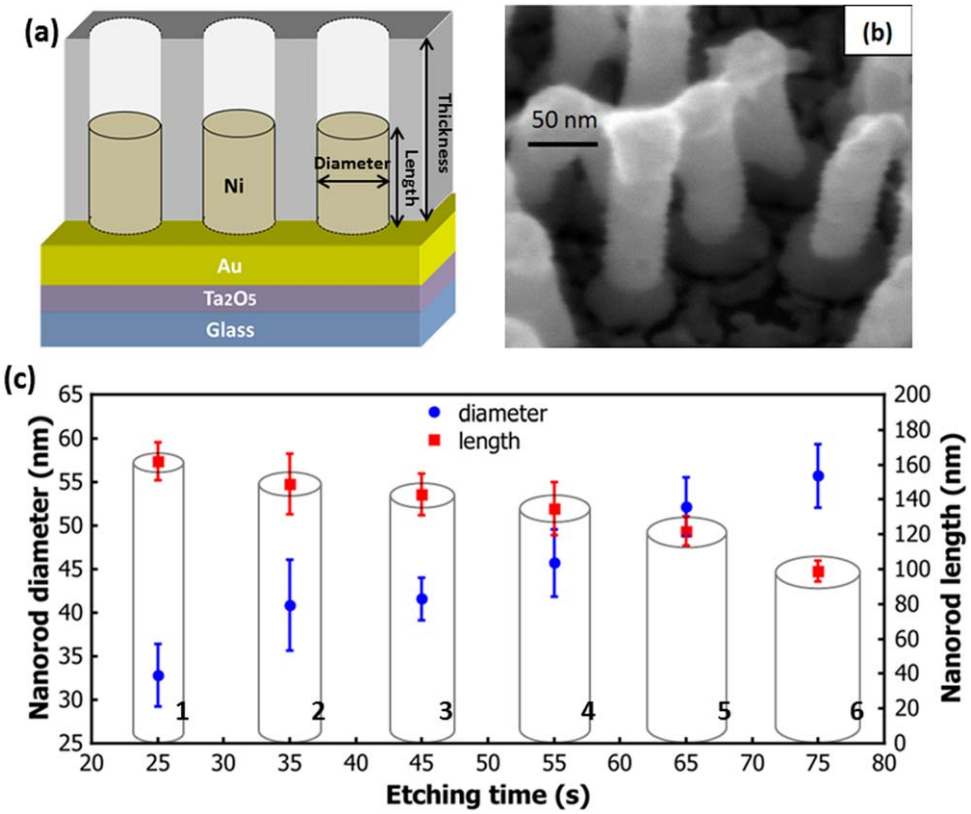


**Figure 1.** (a) Schematic of the Nickel nanorod array embedded in an AAO matrix. (b) SEM image of the nickel nanorod array after removal of the AAO. (c) Dependence of the nanorod diameter as a function of etching time and their corresponding lengths. The aspect ratio decreases from sample 1 to sample 6.

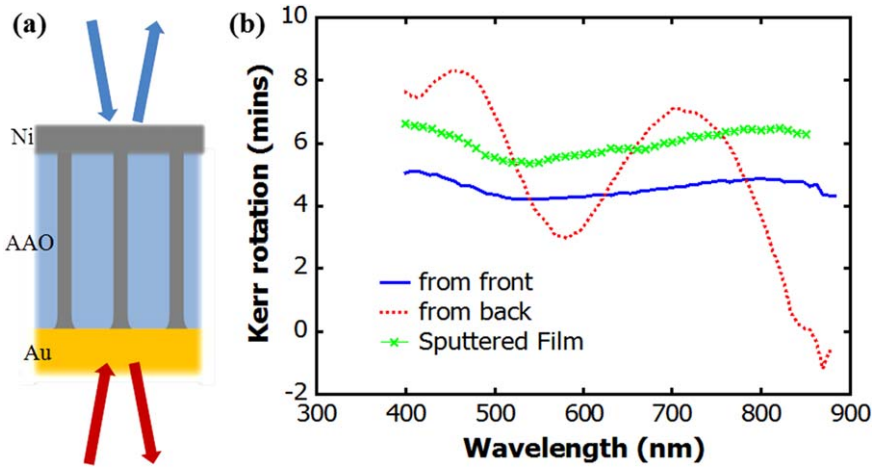


**Figure 2.** (a) Schematic of the MOKE measurements taken from the front (blue arrows) and back side (red arrows) of the overgrown nanorod sample forming a film. (b) Kerr rotation of the sample measured from the front (blue) and back (red), corrected for the rotation due to the glass slide, and the rotation from a sputtered film.

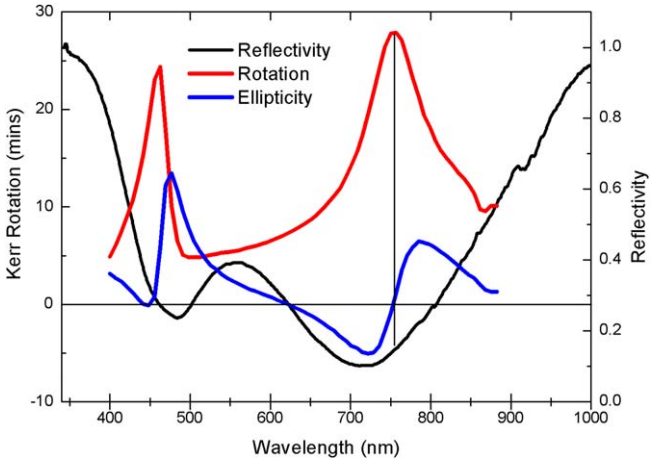


**Figure 3.** Kerr rotation and ellipticity for sample 1, together with reflectivity. Peak rotation corresponds to zero ellipticity and a reflectivity minimum.

## Experimental results

The dramatic effects of a metamaterial can be highlighted with the test structure shown in figure 2. A separate sample (grown as described above) was deliberately overgrown until it formed an optically opaque continuous film along the top of the pores to be used as reference for electrodeposited nickel, figure 2(a). Figure 2(b) shows the Kerr rotation as low valued and featureless across the spectral range when measured from the nickel side, referred to as from the front. However, when measured through the glass (from the back), peaks around 450 nm and 700 nm arise due to the nanostructured geometry. Upon entering the structure through the glass substrate the light experiences multiple internal reflections in the vicinity of the ferromagnetic material. Due to the local time reversal symmetry breaking of the magneto-optical effect, each internal reflection causes a further enhancement of the Kerr rotation at specific wavelengths. When examined from the front, light in this wavelength range cannot penetrate the thick film of nickel to enter the resonance cavity and thus does not provide any MO enhancement. The thick electrodeposited film is equivalent to the polar Kerr rotation at normal incidence in bulk Ni and a similar result is also seen for a thick sputtered film.

For the main sample set, as described in figure 1, we have a two layer composite structure. The bottom layer consists of nickel inclusions in an AAO template and the top layer is AAO with air inclusions. The thin underlayers of gold and tantalum oxide are optically transparent and magneto-optically inactive. Within the template the rods are grown no higher than 40% of the way up the pores of the AAO providing a relatively thick, but influential, layer of non-magnetic material on top. It was found that fully etching a sample after wire growth and removing the AAO template entirely, results in a significant reduction and loss of features in the magneto-optical response. This indicates that the presence of air inclusion layer, and the AAO, strongly influence the optical environment and play an important role in the resonant MO response.

Figure 3 shows a spectroscopic scan of Kerr rotation and ellipticity for sample 1 together with the reflectivity. The plasmonic peak around 450 nm has been previously observed for nickel nanostructures when the dimensions are very much smaller than the wavelength [38]. In our nanorod arrays this feature becomes quickly damped with increasing diameter. This is due

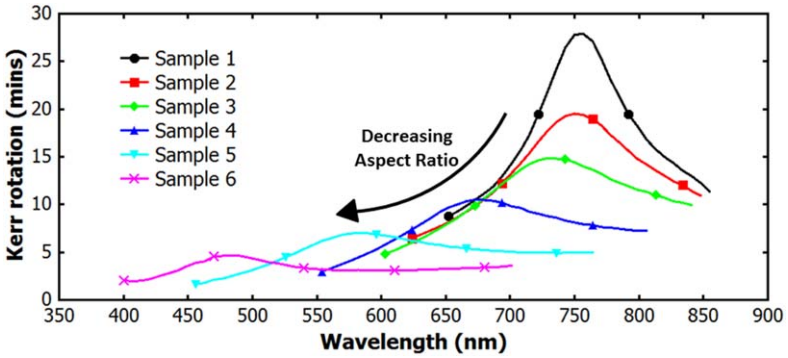


**Figure 4.** Tuneable Kerr rotation as a function of the nanorod geometry and metamaterial layer thickness obtained by increasing the etching time from 25 to 75 s in 10 s intervals.

to increased interaction of the rods, and for the thicker ones which are very close together, this plasmonic effect is gone. All ferromagnetic metals exhibit high damping of their plasmonic resonance owing to the large imaginary part of their dielectric function and high optical absorption over a broad range. Nanostructuring allows access to plasmonic modes but in our sample set, as the gap between rods is reduced, they behave more and more like a thin film and loss components dominate. The second peak at ∼750 nm corresponds to the Fabry-Perot resonance determined by the effective optical parameters of the metamaterial, in this case layer thicknesses [39]. This photonic peak is more easily tuned due to the high degree of freedom when varying the thickness of the thin film template and lengths of the rods. On the other hand, the plasmonic resonance is fixed due to the relatively limited fabrication range for the diameter of the rods.

Crucially, the ellipticity at the point of maximum rotation is zero. This means our structure produces a pure, magneto-optically induced, rotation of the incident linear polarization state on reflection. This results in the highest possible signal to noise ratio for the amount of reflection, and could only be improved upon as reflection approaches zero [40].

Figure 4 shows Kerr rotation vs wavelength and displays the evolution of the photonic MO peak as the overall thickness of the metamaterial and the dimensions of the rods are changed. The plasmonic peak has been removed from this graph for clarity. A blue shift is observed across the sample range, accompanied with a drop in magnitude. The blue shift and damping of the photonic peak is a result of changing the layer thicknesses. As the combined thickness of the two layers is reduced the resonant wavelength becomes shorter. As the thickness of the nickel inclusion layer is reduced further, relative to the thickness of the air inclusion layer, the magneto-optic response becomes damped. Increased rod interaction and the progression of the nickel layer to become more like a thin film also contributes to the observed damping of the photonic peak.

## Simulated results

Effective medium theory was used to further investigate the three competing dynamics at play: changing the diameter of the pores, changing the length of the rods, and changing the total thickness of the sample, and determine the effect of these parameters. Figures 5(a)–(c) show the effect of varying diameter, length and total thickness respectively, independently from the others. It should be noted that for every sample the peak in MO corresponds to a dip in

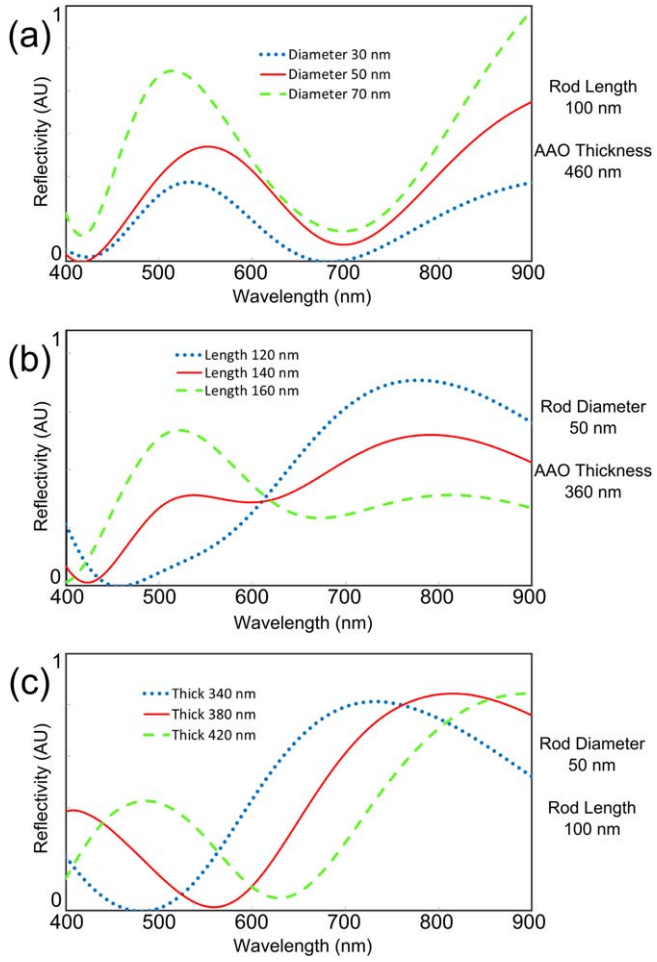


**Figure 5.** Reflectivity curves obtained using Maxwell Garnett Mean Field Theory. Modeling the spectral response as a function of (a) diameter, (b) length and (c) total layer thickness, whilst keeping all other parameters constant.

reflectivity. This is an expected feature of a Fabry-Perot resonator and it is reflectivity that has been modeled. The program was run with two effective medium layers. The first layer has an effective permittivity of the nickel ellipsoids embedded in AAO, including imaginary components, and the second layer is air inclusions in the AAO. The values for the permittivity of nickel used in the simulations were taken from literature [41]. The extremely thin underlayers of gold and tantalum were not included in the simulations.

Looking first at the plasmonic peak, around 400–450 nm. Experimentally the plasmonic peak is only observed for the thinnest rods. As the spacing between adjacent rods is reduced there is increased interaction and damping of the plasmonic mode. This trend is not shown by effective medium theory, which, for these dimensions, can only be considered a first order approximation. Figure 5(a) does show, however, the expected spectral location of the reflectivity minima, and that varying the diameter has no effect on the tuneable photonic resonance.

The evolution of the photonic peak is shown in figure 4 to shift from 750 nm to 480 nm. As shown in figure 5(b), this blue shift arises as a result of decreasing the length of the nanorods. A shift of over 100 nm is observed from the simulations with only a change in length

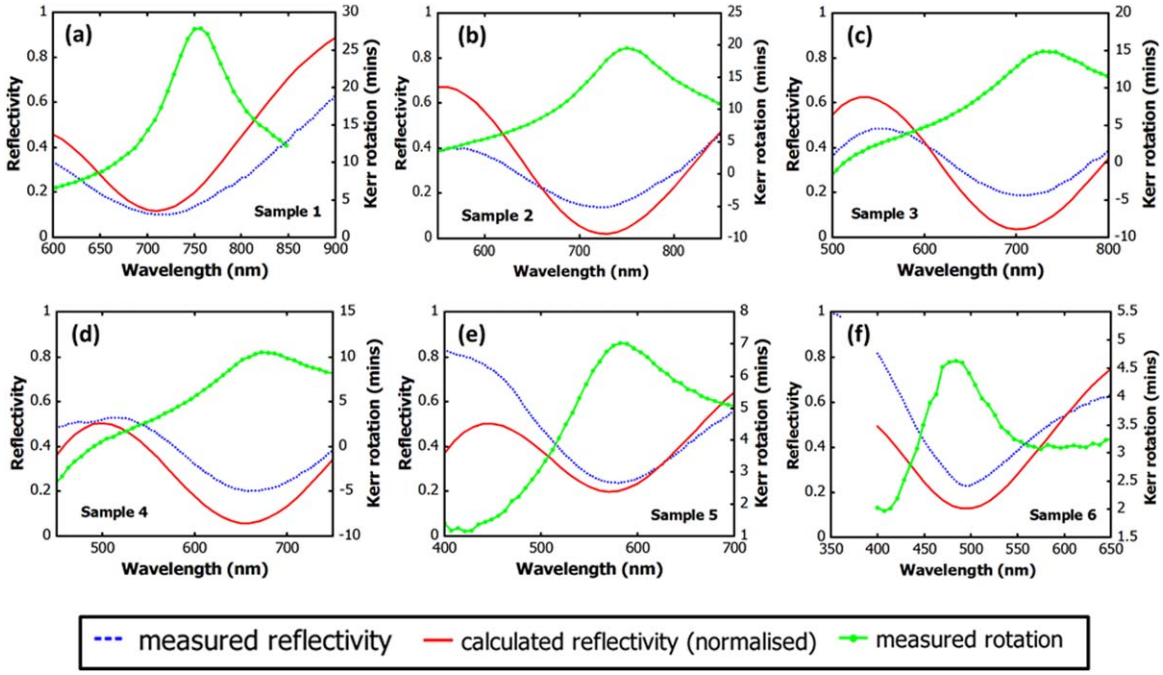


**Figure 6.** Measured and calculated (normalized) reflectivity curves with Kerr rotation for each of the six samples, all at normal incidence. Measured reflectivity was taken relative to an optically thick sputtered nickel film. Calculated curves were obtained using Maxwell Garnett Mean Field Theory and fitted SEM measurements of the samples.

of 40 nm. This demonstrates the sensitivity of the resonance to the thickness of the ferromagnetic layer within our two layer composite metamaterial. A broadening of the photonic peak can also be seen which matches nicely with the damping effects observed in the experimental samples. Reducing the overall thickness of the AAO also contributes to the changing position of the resonance. The values of changing layer thickness in figure 5(c) have been exaggerated for clarity but the blue shift is clear. In our sample set, the thickness of the AAO template is only reduced by 10–15 nm across the range, but when taken in combination, it is enough to amplify the effect of reducing the rod length.

The trends observed in figure 5 are a good indication of how the properties change as one contributing factor is altered at a time and are useful for analysis. We now analyze, in detail, the actual sample set. As a first approach, we considered the geometrical parameters of the structure extracted from SEM images and fine-tuned their value to match the simulations to our measurements. The reflectivity vs wavelength is displayed in figure 6, along with the measured MO spectrum. The measured curves were obtained at normal incidence using a reflection probe, and divided by the spectrum of an optically opaque sputtered nickel film to obtain reflectivity rather than reflectance. It clearly shows that the spectral locations of the calculated reflectivity minima line up extremely well with the measured response. It also demonstrates that the peak MO response closely corresponds to the reflectivity minima.

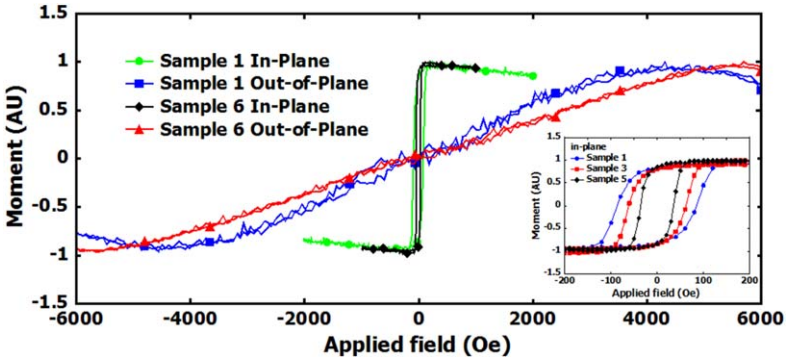


**Figure 7.** VSM measurements showing the in-plane (perpendicular to the rod long axis) and out-of-plane (parallel to the rod long axis) magnetic moments for two representative samples; 1 and 6. The inset shows a close up of the magnetic moment in an in-plane setting showing that the easy axis of magnetization is strongly in plane for all samples, while the coercivity is shown to reduce further with increasing rod diameter as the sample behaves more like a continuous film.

## Magnetic measurements

To complete our analysis, we investigate the magnetic response by acquiring magnetic measurements using vibration sample magnetometry (VSM), both in-plane (perpendicular to the rod long axis) and out-of-plane (parallel to the rod long axis). The results in figure 7 show that as a general trend for all thicknesses, the easy axis of magnetization is in-plane. Along the rod axis the field required for saturation increases with the rod diameter from 4500 to 5700 Oe, whereas from the inset we can see that the in-plane saturation requires less than 150 Oe. The observed reduction in coercivity with increasing diameter in an in-plane setting is to be expected as the reduced gap causes an increased interaction between the rods and the samples behave more and more like a thin film, with the easy axis firmly in-plane. It is this same attribute that results in the damping of the MO modes. For these measurements the air-inclusion layer has no bearing.

The VSM results have confirmed that 0.8 T is more than enough to saturate the samples in any direction—the field used for the MO measurements.

## Conclusion

We have investigated the MO properties of a nickel based metamaterial fabricated by a simple growth technique, and studied the effect of the geometric parameters on the MO response. We demonstrated that the fabrication technique allows us to have accurate control over the dimensions of the nanorods and hence control and tune the properties in the visible regime.

It was found that the samples behaved as sub-wavelength optical cavities with plasmonic and Fabry-Perot type dips in reflectivity at shifting wavelengths depending on the geometry. As the aspect ratio of the nickel rods in the metamaterial was decreased the wavelength(s) at which the magneto-optical Kerr effect was at a maximum blue-shifted and showed a decrease in magnitude.

The behavior and coupling of both optical and magneto-optical properties have been demonstrated and modeled using effective medium theory. Due to the dimensions of the rods

and the sharpness of the MO peak, this nanostructured metamaterial is seen as having great potential for use in devices such as magneto-optical isolators and modulators and for extremely fast, high density magneto-optical storage drives.

## Acknowledgements

The authors acknowledge the Engineering and Physical Sciences Research Council (UK) for financial support.

## References

[1] Smith D R, Padilla W J, Vier D C, Nemat-Nasser S C and Schultz S 2000 *Phys. Rev. Lett.* **84** 4184
[2] Pendry J B 2000 *Phys. Rev. Lett.* **85** 3966
[3] Pollard R J, Murphy A, Hendren W R, Evans P R, Atkinson R, Wurtz G A, Zayats A V and Podolskiy V A 2009 *Phys. Rev. Lett.* **102** 127405
[4] Pendry J B, Schurig D and Smith D R 2006 *Science* **312** 1780
[5] Alù A and Engheta N 2010 *Phys. Rev. Lett.* **105** 263906
[6] Silveirinha M and Engheta N 2006 *Phys. Rev. Lett.* **97** 157403
[7] Engheta N 2007 *Science* **317** 1698
[8] Schurig D, Mock J J, Justice B J, Cummer S A, Pendry J B, Starr A F and Smith D R 2006 *Science* **314** 977
[9] Thurn-Albrecht T, Schotter J, Kästle G A, Emley N, Shibauchi T, Krusin-Elbaum L, Guarini K, Black C T, Tuominen M T and Russell T P 2000 *Science* **290** 2126
[10] Albrecht M, Moser A, Rettner C T, Anders S, Thomson T and Terris B D 2002 *Appl. Phys. Lett.* **80** 3409
[11] Ross C *et al* 2002 *J. Magn. Magn. Mater.* **249** 200
[12] Nasirpouri F, Southern P, Ghorbani M, Iraji zad A and Schwarzacher W 2007 *J. Magn. Magn. Mater.* **308** 35
[13] Evans P R, Yi G and Schwarzacher W 2000 *Appl. Phys. Lett.* **76** 481
[14] Tok J B, Chuang F Y, Kao M C, Rose K A, Pannu S S, Sha M Y, Chakarova G, Penn S G and Dougherty G M 2006 *Angew Chem Int Ed Engl* **45** 6900
[15] Sepúlveda B, Calle A, Lechuga L M and Armelles G 2006 *Opt. Lett.* **31** 1085
[16] Lin Y-C, Kramer C M, Chen C S and Reich D H 2012 *Nanotechnology* **23** 075101
[17] Saib A, Darques M, Piraux L, Vanhoenacker-Janvier D and Huynen I 2005 *IEEE Trans. On Microwave Theory and Tech.* **53** 2043
[18] Encinas A, Demand M, Vila L, Piraux L and Huynen I 2002 *Appl. Phys. Lett.* **81** 2032
[19] Bonanni V, Bonetti S, Pakizeh T, Pirzadeh Z, Chen J, Nogués J, Vavassori P, Hillenbrand R, Åkerman J and Dmitriev A 2011 *Nano Lett.* **11** 5333
[20] Ye X *et al* 2012 *ACS Nano* **6** 2804
[21] Zhang J, Langille M R and Mirkin C A 2011 *Nano Lett.* **11** 2495
[22] Ye X, Zheng C, Chen J, Gao Y and Murray C B 2013 *Nano Lett.* **13** 765
[23] Evans P, Hendren W R, Atkinson R, Wurtz G A, Dickson W, Zayats A V and Pollard R J 2006 *Nanotechnology* **17** 5746
[24] Yin A J, Li J, Jian W, Bennett A J and Xu J M 2001 *Appl. Phys. Lett.* **79** 1039
[25] Metzger R M, Konovalov V V, Sun M, Xu T, Zangari G, Xu B, Benakli M and Doyle W D 2000 *IEEE Trans. Magn.* **36** 30
[26] Ferré R, Ounadjela K, George J M, Piraux L and Dubois S 1997 *Phys. Rev.* B **56** 14066
[27] Haynes C L and Van Duyne R P 2001 *J. Phys. Chem.* B **105** 5599
[28] González-Díaz J B, García-Martín A, García-Martín J M, Cebollada A, Armelles G, Sepúlveda B, Alaverdyan Y and Käll M 2008 *Small* **4** 202
[29] Kanamori Y, Sasaki M and Hane K 1999 *Opt. Lett.* **24** 1422

[30] Leitao D C, Ventura J, Sousa C T, Pereira A M, Sousa J B, Vazquez M and Araujo J P 2011 *Phys. Rev.* B **84** 014410
[31] González-Díaz J B, García-Martín A, Armelles G, Navas D, Vázquez M, Nielsch K, Wehrspohn R B and Gösele U 2007 *Adv. Mater.* **19** 2643
[32] Lin S W, Chang S C, Liu R S, Hu S F and Jan N T 2004 *J. Magn. Magn. Mater.* **282** 28
[33] Samardak A S, Sukovatitsina E V, Ognev A V, Chebotkevich L A, Mahmoodi R, Hosseini M G, Peighambari S M and Nasirpouri F 2011 *Phys. Procedia* **22** 549
[34] Kimel A V, Kirilyuk A, Usachev P A, Pisarev R V, Balbashov A M and Rasing T 2005 *Nature* **435** 655
[35] Hansteen F, Kimel A, Kirilyuk A and Rasing T 2005 *Phys. Rev. Lett.* **95** 047402
[36] Murphy A, Sonnefraud Y, Krasavin A V, Ginzburg P, Morgan F, McPhillips J, Wurtz G, Maier S A, Zayats A V and Pollard R 2013 *Appl. Phys. Lett.* **102** 103103
[37] Einsle J F, Scheunert G, Murphy A, McPhillips J, Zayats A V, Pollard R and Bowman R M 2012 *Nanotechnology* **23** 505302
[38] Chen J *et al* 2011 *Small* **7** 2341
[39] Krutyanskiy V L, Kolmychek I A, Gan'shina E A, Murzina T V, Evans P, Pollard R, Stashkevich A A, Wurtz G A and Zayats A V 2013 *Phys. Rev.* B **87** 035116
[40] Hendren W R, Atkinson R, Pollard R J, Salter I W, Wright C D, Clegg W W and Jenkins D F L 2005 *J. Phys.* D*: Appl. Phys.* **38** 2310
[41] Johnson P B and Christy R W 1974 *Phys. Rev.* B **9** 5056